PROCEEDINGS A

rspa.royalsocietypublishing.org

Research

Cite this article: Gurrutxaga-Lerma B. 2017 Elastodynamic image forces on screw dislocations in the presence of phase boundaries. *Proc. R. Soc. A* **473**: 20170484. http://dx.doi.org/10.1098/rspa.2017.0484

Received: 13 July 2017
Accepted: 17 August 2017

Subject Areas:
materials science, computational mechanics, mechanics

Keywords:
dislocation, edge dislocation, screw dislocation, image force, elastodynamic

Author for correspondence:
Beñat Gurrutxaga-Lerma
e-mail: bg374@cam.ac.uk

Downloaded from https://royalsocietypublishing.org/ on 04 March 2022

Elastodynamic image forces on screw dislocations in the presence of phase boundaries

Beñat Gurrutxaga-Lerma[1,2]

[1]Trinity College Cambridge, University of Cambridge, CB2 1TQ Cambridge, UK
[2]Department of Engineering, University of Cambridge, Trumpington Street, CB2 1QA Cambridge, UK

BG, 0000-0002-3626-963X

The elastodynamic image forces acting on straight screw dislocations in the presence of planar phase boundaries are derived. Two separate dislocations are studied: (i) the injected, non-moving screw dislocation and (ii) the injected (or pre-existing), generally non-uniformly moving screw dislocation. The image forces are derived for both the case of a rigid surface and of a planar interface between two homogeneous, isotropic phases. The case of a rigid interface is shown to be solvable employing Head's image dislocation construction. The case of the elastodynamic image force due to an interface is solved by deriving the reflected wave's contribution to the global solution across the interface. This entails obtaining the fundamental solution (Green's function) for a point unit force via Cagniard's method, and then applying the convolution theorem for a screw dislocation modelled as a force distribution. Complete, explicit formulae are provided when available. It is shown that the elastodynamic image forces are generally affected by retardation effects, and that those acting on the moving dislocations display a dynamic magnification that exceed the attraction (or repulsion) predicted in classical elastostatic calculations.

1. Introduction

The presence of phase boundaries fundamentally conditions the motion and generation of dislocations in crystalline materials. This has a direct impact in the mechanical response of the material, for the interface may act as an insurmountable barrier, thereby contributing to the strain hardening of the original phase [1]; otherwise, the dislocations may be drawn towards the interface, as with diffusional creep [1]. Other situations,

THE ROYAL SOCIETY PUBLISHING

© 2017 The Author(s) Published by the Royal Society. All rights reserved.

Downloaded from https://royalsocietypublishing.org/ on 04 March 2022

such as the behaviour of threading dislocations across epilayers [2,3], or the interaction of dislocations with precipitates [1], are also affected by image forces across the interface that may repel or attract the dislocation.

The conditions upon which a dislocation may display either behaviour depend on the *image forces* that drive them either towards or away from the interface, depending on the nature of the interface and the two phases involved [1]. Shear banding and other interfacial phenomena such as dynamic fracture across phase boundaries typically occur at strain rates high enough that the study of dislocation interactions across and with the interface warrants the use of fully inertial descriptions, as opposed to the traditional quasi-static studies where time is not an explicit variable of the field description.

The image forces receive their name for the *image dislocation* construction, usually attributed to Head [4], that is employed in their derivation when using linear elasticity. According to this construction, the effect an interface has on the dislocation can be construed as the attractive (or repulsive) force a certain image dislocation, lying across the interface, will exert on the actual dislocation. The calculation of the image forces has received ample attention in the past [1]. However, to the author's knowledge, previous work on computing image forces across interfaces have considered only static equilibrium conditions over both the dislocation and its medium.

In [5], the author extended this corpus of results to compute the elastodynamic image forces experienced by dislocations in the presence of a free surface. In that work, the medium was regarded as fully inertial, with time included as an explicit field variable. Although the resulting image forces were shown to eventually converge to the conventional elastostatic image forces, it was shown that the transient state entailed by elastodynamic forces leads to a dynamic magnification of the image forces that persists even at extremely low speeds. In particular, the image force was estimated to be over 40% larger than predicted, for dislocations moving below $50\,\mathrm{m\,s^{-1}}$ after times of the order of 1–10 ns. This would, therefore, condition the interaction between dislocations and free surfaces in ways entirely missed by the conventional elastostatic treatment of the image force problem.

In the light of these results, and given the practical relevance the presence of interfaces has on determining the mechanical behaviour of many crystalline materials, in this article, I focus on deriving the elastodynamic image forces acting on screw dislocations in the presence of (i) a rigid interface, which is done in §2, which will be shown to be amenable to an image dislocation construction, and of (ii) a planar phase boundary across two separate phases, which needs to be tackled differently as done in §3. Both the case of an injected, quiescent (i.e. not-moving, but newly created) screw dislocation and of an injected, non-uniformly moving screw dislocation are considered. Owing to space limitations, the case of an edge dislocation will be the subject of future work. Section 4 offers the main conclusions of this work.

2. Rigid interface

In this section, I consider the case of a right-handed screw dislocation, injected in the immediacy of, or moving towards a phase boundary. As shown in figure 1, the dislocation lies in phase 1, at a distance l from the phase boundary, beyond which lies phase 2. For simplicity, the origin of coordinates is placed at the interface itself, along the epicentral line. The screw dislocation is described as having its cut along the positive x-axis.

(a) Injected, quiescent screw dislocation

Given its greater simplicity, I first study the case of an injected screw dislocation in the immediacy of a rigid boundary. As is shown in figure 1*a*, the dislocation lies in phase 1, while phase 2 is deemed infinitely rigid; this manifests as a boundary condition at the interface specifying that

$$u_z(0, y, t) = 0, \tag{2.1}$$

Downloaded from https://royalsocietypublishing.org/ on 04 March 2022

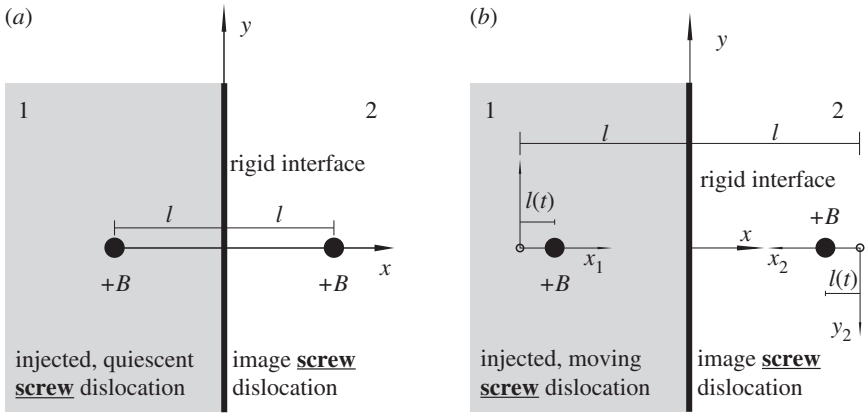

Figure 1. Geometrical of screw dislocations for the derivation of the image forces in the case of a rigid interface. This construction cannot be applied for a general interface.

to wit, that the interface is perfectly reflective. Hereafter, $u_z(x, y, t)$ denotes the out-of-plane displacement field component. The dislocation itself is modelled as a Volterra discontinuity, with its cut surface in the direction of the positive x-axis, so that

$$u_z(x, y, t) = \frac{B}{2} H(x + l) H(t) \delta(y), \tag{2.2}$$

where B is the magnitude of the Burgers vector, $H(\cdot)$ is the Heaviside step function and which describes the screw dislocation as a displacement discontinuity generated at $x = -l$.

The elastodynamic fields of the injected, quiescent screw dislocation in an infinite medium have been derived by Gurrutxaga-Lerma and co-workers in [5,6]. Accordingly, in the absence of a rigid surface, the displacement field corresponding to the dislocation injected at $x = -l$ given by equation (2.2) is

$$u_z^{\text{bulk}}(x, y, t) = \frac{B}{2\pi} \arctan\left[\frac{yt}{(x + l)\sqrt{t^2 - b^2 r_2^2}}\right] H(t - b r_2), \quad r_2^2 = (x + l)^2 + y^2, \tag{2.3}$$

where $b = 1/c_t$ is the transverse slowness of sound, and $c_l = \sqrt{\mu/\rho}$ the transverse speed of sound in an isotropic solid for μ the shear modulus and ρ the density. It must be noted that in [6], I showed that the usual boundary condition with which the injected screw dislocation is modelled (i.e. equation (2.2)) entails an additional emission of a plane wave along the whole cut surface; this emission is a direct result of the way the cut surface is enforced alongside the whole negative half-plane, and it explicitly affects the displacement field alone as

$$u_z^{\text{bulk}}(x, y, t) = \frac{B}{2\pi} \arctan\left[\frac{yt}{(x + l)\sqrt{t^2 - b^2 r^2}}\right] + \underbrace{\frac{B}{2\pi} \text{sign}(x) H(t - by) H(-t + br) H(-x)}_{\text{emission}}. \tag{2.4}$$

Here, I neglect this contribution on three grounds: (i) that the cut surface of the both the bulk and the image dislocation can be chosen in such a way that it does not cut the interface; (ii) that the emission may be made to vanish if the boundary condition modelling the injection is such that the cut surface itself propagates outwards from the injection site at the shear speed of sound and (iii) that otherwise the emission of the bulk dislocation will be cancelled by that of the image dislocation because it changes signs across the cut. Furthermore, the emission vanishes identically upon computing the stress and strain fields, thereby not affecting the image forces.

The boundary condition established by equation (2.1) may, therefore, be satisfied as in the static case [1], via the image dislocation construction shown in figure 1*a*: an image dislocation of

Downloaded from https://royalsocietypublishing.org/ on 04 March 2022

the same sign, located at a distance l away from the surface, is such that

$$\begin{aligned} u_z^{\text{tot}}(x,y,t) &= u_z^{\text{bulk}} + u_z^{\text{image}} \\ &= \frac{B}{2\pi}\left[\arctan\left[\frac{yt}{(x+l)\sqrt{t^2-b^2((x+l)^2+y^2)}}\right]\right. \\ &\quad \left. + \arctan\left[\frac{yt}{(x-l)\sqrt{t^2-b^2((x-l)^2+y^2)}}\right]\right]. \end{aligned} \tag{2.5}$$

Clearly, when $x=0$ (i.e. at the interface),

$$u_z^{\text{tot}}(x,y,t) = \frac{B}{2\pi}\left[\arctan\left[\frac{yt}{l\sqrt{t^2-b^2(l^2+y^2)}}\right] + \arctan\left[\frac{yt}{-l\sqrt{t^2-b^2(l^2+y^2)}}\right]\right] = 0. \tag{2.6}$$

Thus, the image and bulk dislocation's stress fields are (q.v. [5,6])

$$\sigma_{yz}^{\text{image}} = \frac{\mu B}{2\pi}\frac{t(x-l)(t^2-b^2((x-l)^2+2y^2))}{r_2^2(t^2-b^2y^2)\sqrt{t^2-b^2r_2^2}}H(t-br_2), \quad r_2^2=(x-l)^2+y^2, \tag{2.7}$$

$$\sigma_{yz}^{\text{bulk}} = \frac{\mu B}{2\pi}\frac{t(x+l)(t^2-b^2((x+l)^2+2y^2))}{r_1^2(t^2-b^2y^2)\sqrt{t^2-b^2r_2^2}}H(t-br_1), \quad r_1^2=(x+l)^2+y^2, \tag{2.8}$$

$$\sigma_{xz}^{\text{image}} = -\frac{\mu B}{2\pi}\frac{ty}{r_2^2\sqrt{t^2-b^2r_2^2}}H(t-br_2), \quad r_2^2=(x-l)^2+y^2 \tag{2.9}$$

and

$$\sigma_{xz}^{\text{bulk}} = -\frac{\mu B}{2\pi}\frac{ty}{r_1^2\sqrt{t^2-b^2r_1^2}}H(t-br_1), \quad r_1^2=(x+l)^2+y^2. \tag{2.10}$$

Whereupon the total stress field is

$$\begin{aligned} \sigma_{xz}(x,y,t) &= \sigma_{xz}^{\text{image}} + \sigma_{xz}^{\text{bulk}} \\ &= -\frac{\mu B}{2\pi}\left[\frac{ty}{r_1^2\sqrt{t^2-b^2r_1^2}}H(t-br_1) + \frac{ty}{r_2^2\sqrt{t^2-b^2r_2^2}}H(t-br_2)\right] \end{aligned} \tag{2.11}$$

and

$$\begin{aligned} \sigma_{yz}(x,y,t) &= \sigma_{yz}^{\text{image}} + \sigma_{yz}^{\text{bulk}} \\ &= \frac{\mu B}{2\pi}\left[\frac{t(x+l)(t^2-b^2((x+l)^2+2y^2))}{r_1^2(t^2-b^2y^2)\sqrt{t^2-b^2r_2^2}}H(t-br_1)\right. \\ &\quad \left. + \frac{t(x-l)(t^2-b^2((x-l)^2+2y^2))}{r_2^2(t^2-b^2y^2)\sqrt{t^2-b^2r_2^2}}H(t-br_2)\right]. \end{aligned} \tag{2.12}$$

Hence, the image force is given by

$$F_x(t) = \sigma_{yz}^{\text{image}}B = -\frac{\mu B^2}{4\pi}\frac{\sqrt{t^2-4b^2l^2}}{lt}H(t-2bl). \tag{2.13}$$

Downloaded from https://royalsocietypublishing.org/ on 04 March 2022

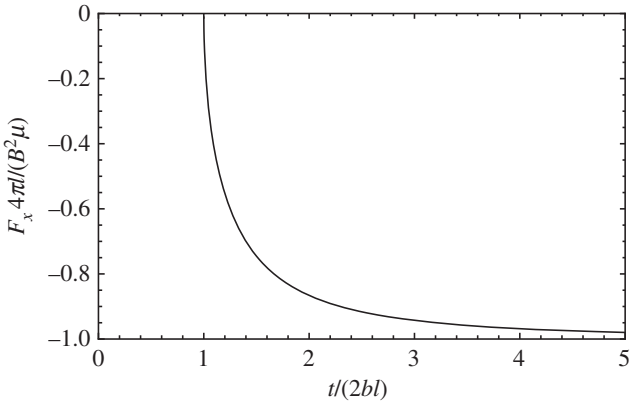

Figure 2. Evolution of the magnitude of the image force with time.

Writing $\tau = t/2bl$, the effect the time-dependent elastodynamic fields have over the image force may be better appreciated:

$$F_x(\tau) = -\frac{\mu B^2}{4\pi}\left[\frac{1}{l}\right]\underbrace{\left[\frac{\sqrt{\tau^2-1}}{\tau}H(\tau-1)\right]}_{\text{dynamic contribution}}. \tag{2.14}$$

The factor in the second bracket corresponds with the elastodynamic contribution to the image force, which in this case is presented as a strong transient decaying towards the static solution [1], which is in fact recovered in the $t \to \infty$ limit[1] as

$$\lim_{t\to\infty} -\frac{\mu B^2}{4\pi}\frac{\sqrt{t^2-4b^2l^2}}{lt}H(t-2bl) = -\frac{\mu B^2}{4\pi}\frac{1}{l}. \tag{2.15}$$

The image force for this case is represent in figure 2, which shows that the image force has three distinct behaviours: (i) between the injection at $t = 0$ and $t = 2bl$ the dislocation does not experience an image force at all; (ii) upon the arrival of the reflected wave at $t = 2bl$ (which is approx. 1 ns for a dislocation lying a few micrometres away from the interface in a typical metal), the dislocation experiences a repulsive image force of increasing magnitude up to about $t \approx 5bl$; when (iii) the image force saturates towards the elastostatic value.

(b) Injected, moving dislocation

Given that the boundary condition at the interface remains the same, i.e. the interface acts as a reflective wall via equation (2.1), the image dislocation construction required in this case is analogous to that of the quiescent dislocation's case, with the exception that in this case both the bulk dislocation and its image will approach the rigid surface. In order to prove this, one first needs to provide the u_z displacement field component for the bulk dislocation that, being injected at some distance l from the interface, moves non-uniformly according to some past history function $l = l(t)$ towards the surface.

In the following, I derive the form of the displacement field component and then proceed to find the form of both the stress fields and the image force.

[1]Given that the elastostatic solution is achieved once the elastic field has propagated to $r \to \infty$, it may also be obtained by letting $\rho \to 0$ at any one time, since that would define a medium where waves propagate infinitely quickly.

Downloaded from https://royalsocietypublishing.org/ on 04 March 2022

(i) Displacement field of an injected, non-uniformly moving screw dislocation

Under plane strain conditions, owing to the cylindrical symmetry of the screw dislocation the governing equation may be reduced to

$$\frac{\partial^2 u_z}{\partial x^2} + \frac{\partial^2 u_z}{\partial y^2} = b^2 \frac{\partial^2 u_z}{\partial t^2}, \tag{2.16}$$

which denotes that the material is modelled as being subjected to antiplane shear alone [1]. Other loading situations such as pure plane strain cannot be modelled employing equation (2.16) alone.

The dislocation is modelled in the sense of Volterra, so that the boundary condition is

$$u_z(x,0,t) = \frac{B}{2} H(l(t) - x) H(t) \equiv \frac{B}{2} H(\eta(x) - t) H(t), \tag{2.17}$$

where $\eta(x) = l^{-1}(t)$ is the inverse of the past history function.

For mathematical convenience, I rewrite this boundary condition (q.v. [7,8]) as the superposition of the following two:

(i) An injection contribution, which was solved in [5] and its expression given in §2a

$$u_z(x,0,t) = \frac{B}{2} H(x) H(t). \tag{2.18}$$

(ii) A mobile contribution

$$u_z(x,0,t) = \frac{B}{2} [H(\eta(x) - t) - H(x)] H(t). \tag{2.19}$$

The solution procedure follows the usual Cagniard–de Hoop method [5,6,9]. Define the following successive Laplace transforms

$$\hat{f}(x,y,s) = \int_0^\infty f(x,y,t)\, \mathrm{e}^{-st}\, \mathrm{d}t \quad \text{and} \quad F(\lambda,y,s) = \int_{-\infty}^\infty \hat{f}(x,y,s)\, \mathrm{e}^{-\lambda s x}\, \mathrm{d}x, \tag{2.20}$$

which upon being applied to equation (2.16), lead to the following equation in Laplace space

$$\beta^2 s^2 U_z = \frac{\partial^2 U_z}{\partial y^2}, \quad \text{with } \beta^2 = b^2 - \lambda^2. \tag{2.21}$$

Assuming that the solution is stable,[2] it will be of the form

$$U_z(\lambda,y,s) = C(\lambda,s)\, \mathrm{e}^{-s\beta y}, \tag{2.22}$$

where $C(\lambda,s)$ is an integration constant, which can be found from the boundary condition, whereupon

$$U_z(\lambda,y,s) = -\frac{B}{2s} \left[\int_0^\infty \mathrm{e}^{-s(\eta(\xi) - \lambda\xi)}\, \mathrm{d}\xi \right] \mathrm{e}^{-s\beta y}. \tag{2.23}$$

The inversion of U_z is performed using the Cagniard–de Hoop technique. Inverting the spatial variable

$$\hat{u}_z(x,y,s) = \frac{1}{2\pi \mathrm{i}} \int_{-\mathrm{i}\infty}^{\mathrm{i}\infty} \frac{-B}{2} \left[\int_0^\infty \mathrm{e}^{-s(\eta(\xi) - \lambda\xi)}\, \mathrm{d}\xi \right] \mathrm{e}^{-s(\beta y - \lambda x)}\, \mathrm{d}\lambda. \tag{2.24}$$

Reorganizing

$$\hat{u}_z(x,y,s) = \frac{-B}{2} \int_0^\infty \mathrm{d}\xi\, \mathrm{e}^{-s\eta(\xi)} \frac{1}{2\pi \mathrm{i}} \int_{-\mathrm{i}\infty}^{\mathrm{i}\infty} \mathrm{d}\lambda\, \mathrm{e}^{-s(\beta y - \lambda(x-\xi))}. \tag{2.25}$$

The integral in λ may be rewritten as an integral in $\tau = \beta y - \lambda \tilde{x}$, with $\tilde{x} = x - \xi$, by adequately distorting the integration path into a Cagniard path along the hyperbola branches prescribed

[2]That is, that $\lim_{y\to\infty} U_Z = 0$.

Downloaded from https://royalsocietypublishing.org/ on 04 March 2022

by $\lambda_\pm$. This results in the inversion integral written in Cagniard form as

$$\hat{u}_z(x,y,s) = \frac{-B}{2\pi}\int_0^\infty \mathrm{e}^{-s\tilde{\tau}}\,\mathrm{d}\tau \int_0^\infty H(\tilde{\tau}-b\tilde{r})\mathrm{Im}\left[\frac{\partial\lambda_+}{\partial\tau}\right]\mathrm{d}\xi, \tag{2.26}$$

where $\tilde{\tau}=\tau-\eta(\xi)$, $\tilde{r}^2=\tilde{x}^2+y^2$. Upon inverting in time via the Bromwich integral, the following mobile field is obtained by inspection

$$u_z(x,y,t) = \frac{-B}{2\pi}\int_0^\infty H(\tilde{t}-b\tilde{r})\frac{\tilde{t}y}{\tilde{r}^2\sqrt{\tilde{t}^2-b^2\tilde{r}^2}}\,\mathrm{d}\xi. \tag{2.27}$$

The corresponding stress fields are given in [5]:

$$\sigma_{yz}(x,y,t) = \frac{\mu B}{2\pi}\frac{\partial}{\partial t}\int_0^\infty H(\tilde{t}-b\tilde{r})\frac{\tilde{t}^2(\tilde{x}^2-y^2)-b^2\tilde{r}^2\tilde{x}^2}{\tilde{r}^4\sqrt{\tilde{t}^2-b^2\tilde{r}^2}}\,\mathrm{d}\xi \tag{2.28}$$

and

$$\sigma_{xz}(x,y,t) = -\frac{\mu B}{2\pi}\frac{\partial}{\partial t}\int_0^\infty H(\tilde{t}-b\tilde{r})\frac{\tilde{x}y(b^2\tilde{r}^2-2\tilde{t}^2)}{\tilde{r}^4\sqrt{\tilde{t}^2-b^2\tilde{r}^2}}\,\mathrm{d}\xi. \tag{2.29}$$

These expressions must then be superimposed with the injected (or pre-existing) dislocation's field components to obtain the full field description of an injected (or pre-existing), non-uniformly moving dislocation.

Both equation (2.27) (and equations (2.28) and (2.29)) describe a dislocation that is injected at the origin and moves according to $\eta(x)$, along the positive x-axis. The image dislocation construction will consist of a like-signed screw dislocation moving towards the bulk dislocation with the same past history. However, given that the mobile fields are not symmetrical any longer, in order to preserve the convention upon which equation (2.27) has been derived, here I use the image dislocation construction shown in figure 1*b*. The general coordinate axis is located at the rigid interface, along the epicentral line. The bulk dislocation is located at $x=-l$ at $t=0$, and starts to move along the positive direction of the local x_1-axis with a past history function $x_1=l(t)$. Here $x_1=x+l$, and $y_1=y$. The image dislocation is a positive screw dislocation that moves in the positive direction of the x_2-axis with the same mobility law $x_2=l(t)$; however, here the local coordinate system is $x_2=-x+l$, $y_2=-y$.

Thus, the total displacement field at $x=0$ will be

$$\begin{aligned} u_z^{\mathrm{tot}}(0,y,t) &= u_z^{\mathrm{bulk}}(0,y,t)+u_z^{\mathrm{im}}(0,y,t)\\ &= \frac{-B}{2\pi}\left[\int_0^\infty H(\tilde{t}-b\tilde{r}_1)\frac{\tilde{t}y}{\tilde{r}_1^2\sqrt{\tilde{t}^2-b^2((l+\xi)^2+y^2)}}\,\mathrm{d}\xi\right.\\ &\quad\left.+\int_0^\infty H(\tilde{t}-b\tilde{r}_2)\frac{-\tilde{t}y}{\tilde{r}_2^2\sqrt{\tilde{t}^2-b^2((l+\xi)^2+y^2)}}\,\mathrm{d}\xi\right]=0, \end{aligned} \tag{2.30}$$

since $\tilde{r}_1=\sqrt{\tilde{x}_1^2+y_1^2}$, $\tilde{r}_2=\sqrt{\tilde{x}_2^2+y_2^2}$ and $\tilde{r}_1|_{x=0}=\tilde{r}_2|_{x=0}=\sqrt{(l+\xi)^2+y^2}$.

Having proven that the image dislocation construction is valid for a moving dislocation, the stress fields can be written as

$$\begin{aligned} \sigma_{yz}^{\mathrm{tot}} = \frac{\mu B}{2\pi}\frac{\partial}{\partial t}\left[\int_0^\infty H(\tilde{t}-b\tilde{r}_1)\frac{\tilde{t}^2((x+l-\xi)^2-y^2)-b^2\tilde{r}_1^2(x+l-\xi)^2}{\tilde{r}_1^4\sqrt{\tilde{t}^2-b^2\tilde{r}_1^2}}\,\mathrm{d}\xi\right.\\ \left.+\int_0^\infty H(\tilde{t}-b\tilde{r}_2)\frac{\tilde{t}^2((-x+l-\xi)^2-y^2)-b^2\tilde{r}_2^2(-x+l-\xi)^2}{\tilde{r}_2^4\sqrt{\tilde{t}^2-b^2\tilde{r}_2^2}}\,\mathrm{d}\xi\right] \end{aligned} \tag{2.31}$$

Downloaded from https://royalsocietypublishing.org/ on 04 March 2022

and

$$\sigma_{xy}^{\text{tot}} = -\frac{\mu B}{2\pi}\frac{\partial}{\partial t}\left[\int_0^\infty H(\tilde{t}-b\tilde{r}_1)\frac{(x+l-\xi)y(b^2\tilde{r}^2-2\tilde{t}^2)}{\tilde{r}_1^4\sqrt{\tilde{t}^2-b^2\tilde{r}_1^2}}\,\mathrm{d}\xi \right.$$
$$\left. -\int_0^\infty H(\tilde{t}-b\tilde{r}_2)\frac{(-x+l-\xi)y(b^2\tilde{r}_2^2-2\tilde{t}^2)}{\tilde{r}_2^4\sqrt{\tilde{t}^2-b^2\tilde{r}_2^2}}\,\mathrm{d}\xi\right]. \tag{2.32}$$

As stated before, these field components must be superimposed with either the injected contribution (or the pre-existing, elastostatic field) of a dislocation of opposite sign, in order to recover the full-field solution of the injected (or pre-existing) and non-uniformly moving dislocation's.

The resulting image force will there for the non-uniformly moving and uniformly moving case are as follows:

$$F_x(t) = \sigma_{yz}^{\text{im}}|_{x=-l,y=0}B = \frac{\mu B^2}{2\pi}\frac{\partial}{\partial t}\int_0^\infty H(\tilde{t}-b|2l-\xi|)\frac{\sqrt{\tilde{t}^2-b^2(2l-\xi)^2}}{(2l-\xi)^2}\,\mathrm{d}\xi$$
$$-\frac{\mu B^2}{4\pi}\frac{t}{l\sqrt{t^2-4b^2l^2}}H(t-2bl)$$
$$=\frac{\mu B^2}{2\pi}\int_0^\infty H(\tilde{t}-b|2l-\xi|)\frac{\tilde{t}}{(2l-\xi)^2\sqrt{\tilde{t}^2-b^2(2l-\xi)^2}}\,\mathrm{d}\xi$$
$$-\frac{\mu B^2}{4\pi}\frac{t}{l\sqrt{t^2-4b^2l^2}}H(t-2bl). \tag{2.33}$$

The particular case when the dislocation moves uniformly merits some consideration to clarify what equation (2.33) entails. Therefore, let $\eta(\xi) = d\cdot\xi$, where $d = 1/v_{\text{glide}} = \text{const.}$ is the slowness with which the screw dislocation glides uniformly. That the image dislocation construction is valid is ensured by the fact that equation (2.30) trivially contains the case when $\eta(\xi) = d\cdot\xi$. The image fields will then be

$$\sigma_{yz}^{\text{tot}} = \frac{\mu B}{2\pi}\left[\frac{t^3x_1+dt^2(y^2-x_1^2)-b^2tx_1(x_1^2+2y^2)+b^2dr_1^2x_1^2}{r_1^2\sqrt{t^2-b^2r_1^2}(t^2-2dtx_1-b^2y^2+d^2r_1^2)}H(t-br_1)\right.$$
$$\left.+\frac{t^3x_2+dt^2(y^2-x_2^2)-b^2tx_2(x_2^2+2y^2)+b^2dr_2^2x_2^2}{r_2^2\sqrt{t^2-b^2r_2^2}(t^2-2dtx_2-b^2y^2+d^2r_2^2)}H(t-br_2)\right] \tag{2.34}$$

and

$$\sigma_{xy}^{\text{tot}} = \frac{\mu B}{2\pi}\left[\frac{y(t^3-2dt^2x_1-b^2ty^2+b^2dr_1^2x_1)}{r_1^2\sqrt{t^2-b^2r_1^2}(t^2-2dtx_1-b^2y^2+d^2r_1^2)}H(t-br_1)\right.$$
$$\left.-\frac{y(t^3-2dt^2x_2-b^2ty^2+b^2dr_2^2x_2)}{r_2^2\sqrt{t^2-b^2r_2^2}(t^2-2dtx_2-b^2y^2+d^2r_2^2)}H(t-br_2)\right], \tag{2.35}$$

where again $x_1 = x+l$, $x_2 = -x+l$, $r_1 = \sqrt{x_1^2+y^2}$ and $r_2 = \sqrt{x_2^2+y^2}$. Again, these fields must be superimposed to the injected dislocation's.

The image force for the injected, uniformly moving dislocation will, therefore, be

$$F_x(t) = -\frac{\mu B^2}{4\pi}\frac{d\sqrt{t^2-4b^2l^2}}{2dlt-t^2}H(t-2bl) \tag{2.36}$$

Downloaded from https://royalsocietypublishing.org/ on 04 March 2022

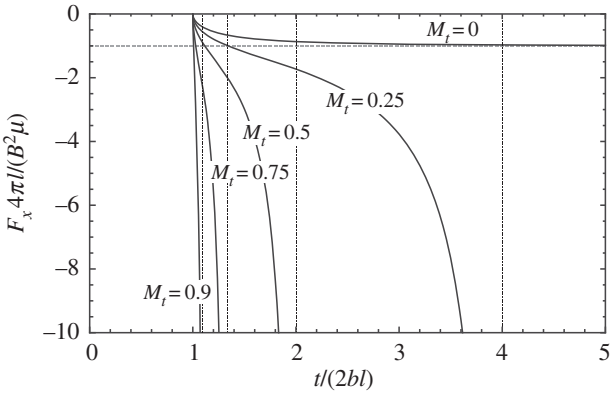

Figure 3. Evolution of the magnitude of the image force with time for a uniformly moving screw dislocation at different M_t. The vertical lines signify the instant in time when the dislocation reaches the interface.

or in terms of the non-dimensional variables $\tau = t/2bl$ and the transverse Mach number $M_t = b/d$

$$F_x(t) = -\frac{\mu B^2}{2\pi}\left[\frac{1}{2l}\right]\underbrace{\left[\frac{\sqrt{\tau^2-1}}{\tau - M_t\tau^2}H(\tau-1)\right]}_{\text{dynamic contribution}}. \tag{2.37}$$

The resulting $F_x(t)$ is shown in figure 3. As can be seen, the quiescent case is recovered when $M_t \to 0$. As in the quiescent case, the dislocation does not experience a repulsive image force until the reflected wave has had enough time to reach the dislocation anew, at $\tau = 2bl$. Once this happens, the image force increases in magnitude, but unlike in the quiescent case, it does not saturate but tends to grow to the point of divergence when the dislocation reaches the rigid boundary. Thus, the image force is expected to be of much larger magnitude than the one predicted with elastostatics. This is solely due to the dynamic contribution highlighted on equation (2.37). The significance of this magnification cannot be overstated: a dislocation located 1 µm away from the interface, and moving at $20\,\mathrm{m\,s^{-1}}$ towards it, will after 1 ns experience a repulsive image force that is 40% larger than its elastostatic counterpart.

3. Two phases

Consider now the case where a screw dislocation lies at some distance l from the interface between phase 1 (where the material is injected in), and phase 2, as is shown in figure 4. Phase 1 is defined by the elastic constants Λ_1 and μ_1 for Lamé's first and second parameter, ρ_1 for the density and $b_1 = 1/c_{t_1} = \sqrt{\rho_1/\mu_1}$ for the shear slowness of sound. Analogously, phase 2 is defined by the elastic constants Λ_2 and μ_2, ρ_2, and $b_2 = 1/c_{t_2} = \sqrt{\rho_2/\mu_2}$. The boundary conditions require that displacements be compatible and that the tractions be continuous across the interface (i.e. that the materials be welded at the interface):

$$u_z^{(1)}(0, y, t) = u_z^{(2)}(0, y, t) \tag{3.1}$$

and

$$\sigma_{xz}^{(1)}(0, y, t) = \sigma_{xz}^{(2)}(0, y, t). \tag{3.2}$$

The boundary conditions cannot simply be satisfied by invoking an image dislocation construction such as the one used in §2a,b—the interface acts as an acoustic refraction boundary, and the acoustic impedances of the media are not necessarily the same. However,

Downloaded from https://royalsocietypublishing.org/ on 04 March 2022

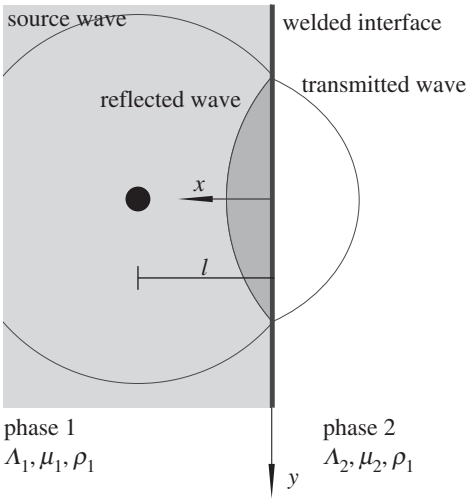

Figure 4. Screw dislocation located in phase 1 at a distance *l* from the interface. The dislocation can be regarded as a source of waves, that will be reflected and transmitted upon being scattered by the interface.

the problem can still be solved through similar means, by treating the screw dislocation as a source of antiplane elastic waves [9] that will be reflected by and transmitted across the interface. The wave component that is reflected back into phase 1 is the one responsible for the image force.

In order to solve this problem, I will therefore first find the the fundamental solution for a force line source located in phase 1. Then I will invoke the linearity of the medium to find the reflected elastodynamic field of the dislocation, which immediately leads to the image force.

(a) Fundamental solution to a line source

The response of phase 1 is governed by

$$\frac{\partial^2 u_z^{(1)}}{\partial x^2} + \frac{\partial^2 u_z^{(1)}}{\partial y^2} = b_1^2 \frac{\partial^2 u_z^{(1)}}{\partial t^2}. \tag{3.3}$$

The medium is excited by a source of the form

$$u_z^{(1)}(x, y, t) = \delta(x - x_0)\delta(y - y_0)\delta(t - t_0), \tag{3.4}$$

where $\delta(\cdot)$ is Dirac's delta function, and which describes a line source located at (x_0, y_0) on phase 1 and acting at time t_0. Note that this does not model a dislocation, but a point source. This source term is a unitary force proper, so that to all effects, equation (3.3) may be rewritten as

$$\frac{\partial^2 u_z^{(1)}}{\partial x^2} + \frac{\partial^2 u_z^{(1)}}{\partial y^2} - b_1^2 \frac{\partial^2 u_z^{(1)}}{\partial t^2} = \frac{1}{\mu_1}\delta(x - x_0)\delta(y - y_0)\delta(t - t_0). \tag{3.5}$$

The response of phase 2 is governed by

$$\frac{\partial^2 u_z^{(2)}}{\partial x^2} + \frac{\partial^2 u_z^{(2)}}{\partial y^2} = b_2^2 \frac{\partial^2 u_z^{(2)}}{\partial t^2}. \tag{3.6}$$

Both media are coupled via equations (3.1) and (3.2), which define a welded interface.

Downloaded from https://royalsocietypublishing.org/ on 04 March 2022

In order to study this problem, I define the following integral transforms, applied in succession:

$$\hat{f}(x,y,s)=\int_0^\infty f(x,y,t)\,\mathrm{e}^{-st}\,\mathrm{d}t,\quad F(k_x,k_y,s)$$
$$=\int_{-\infty}^{\infty}\mathrm{d}x\int_{-\infty}^{\infty}\mathrm{d}y\,\hat{f}(x,y,s)\,\mathrm{e}^{-\mathrm{i}(k_x x+k_y y)}. \tag{3.7}$$

Transforming equation (3.3) leads to

$$U_z^{(1,S)}(k_x,k_y,s)=\frac{1}{\mu_1}\frac{\mathrm{e}^{-st_0-\mathrm{i}(k_x x_0+k_y y_0)}}{k_x^2+k_y^2+s^2b_1^2}, \tag{3.8}$$

where the superindex S denotes that this is the source term in the Laplace–Fourier space.

The first inversion in x may be solved invoking Cauchy's residue theorem (and Jordan's lemma):

$$\mu_1 U_z^{(1,S)}(x,k_y,s)=\frac{1}{2\pi}\int_{-\infty}^{\infty}\frac{\mathrm{e}^{-st_0-\mathrm{i}(k_x x_0+k_y y_0)}}{k_x^2+k_y^2+s^2b_1^2}\mathrm{e}^{\mathrm{i}k_x x}\,\mathrm{d}k_x$$
$$=\mathrm{e}^{-st_0-\mathrm{i}k_y y_0}\left[\frac{1}{2\pi}\int_{-\infty}^{\infty}\frac{\mathrm{e}^{-\mathrm{i}k_x(x_0-x)}}{\left(k_x+\mathrm{i}\sqrt{k_y^2+b_1^2s^2}\right)\left(k_x-\mathrm{i}\sqrt{k_y^2+b_1^2s^2}\right)}\right]$$
$$=\mathrm{e}^{-st_0-\mathrm{i}k_y y}\mathrm{Res}\left[\frac{\mathrm{e}^{-\mathrm{i}k_x(x_0-x)}}{\left(k_x+\mathrm{i}\sqrt{k_y^2+b_1^2s^2}\right)\left(k_x-\mathrm{i}\sqrt{k_y^2+b_1^2s^2}\right)}\right]_{k_x=\mathrm{i}\sqrt{k_y^2+b_1^2s^2}}$$
$$=\frac{1}{2}\mathrm{e}^{-st_0-\mathrm{i}k_y y_0}\frac{\mathrm{e}^{-\sqrt{k_y^2+b_1^2s^2}(x-x_0)}}{\sqrt{k_y^2+b_1^2s^2}}. \tag{3.9}$$

The inversion in y is

$$\mu_1 U_z^{(1,S)}(x,y,s)=\frac{1}{2\pi}\int_{-\infty}^{\infty}\frac{1}{2}\,\mathrm{e}^{-st_0-\mathrm{i}k_y y_0}\frac{\mathrm{e}^{-\sqrt{k_y^2+b_1^2s^2}(x-x_0)}}{\sqrt{k_y^2+b_1^2s^2}}\,\mathrm{e}^{\mathrm{i}k_y y}\,\mathrm{d}k_y. \tag{3.10}$$

This integral may be rewritten in the same form used in §2a,b when discussing the Cagniard–de Hoop inversion, by setting $k_y=\mathrm{i}s\lambda$, whereupon

$$\mu_1 U_z^{(1,S)}(x,y,s)=\frac{1}{2\pi\mathrm{i}}\int_{-\mathrm{i}\infty}^{\mathrm{i}\infty}\frac{\mathrm{e}^{-s(t_0+\beta_1(x-x_0)+\lambda(y-y_0)}}{2\beta_1}\,\mathrm{d}\lambda$$
$$=\frac{1}{2\pi\mathrm{i}}\int_{-\mathrm{i}\infty}^{\mathrm{i}\infty}U_{1,S}\,\mathrm{e}^{-s(\lambda y+\beta_1(x-x_0))}\,\mathrm{d}\lambda, \tag{3.11}$$

where $\beta_1^2=b_1^2-\lambda^2$ and

$$U_{1,S}=\frac{\mathrm{e}^{-s(t_0-\lambda y_0)}}{2\beta_1}.$$

Upon reaching the interface at $x=0$, the source term will be scattered, leading to a reflected wave in phase 1, and to a wave transmitted into phase 2 [9]. Without loss of generality, these reflected $U_z^{(1,R)}$ and transmitted $U_z^{(2,T)}$ terms may be written as being of the form (cf. [9]):

$$\mu_1 U_z^{(1,R)}=\frac{1}{2\pi\mathrm{i}}\int_{-\mathrm{i}\infty}^{\mathrm{i}\infty}U_{1,R}\,\mathrm{e}^{-s(\lambda y+\beta_1(x+x_0))}\,\mathrm{d}\lambda \tag{3.12}$$

and

$$\mu_1 U_z^{(2,T)}=\frac{1}{2\pi\mathrm{i}}\int_{-\mathrm{i}\infty}^{\mathrm{i}\infty}U_{2,T}\,\mathrm{e}^{-s(\lambda y+\beta_2 x+\beta_1 x_0)}\,\mathrm{d}\lambda. \tag{3.13}$$

Downloaded from https://royalsocietypublishing.org/ on 04 March 2022

The coefficients $U_{1,R}$ and $U_{2,T}$ can then be found by imposing the compatibility conditions at the interface, $x=0$. The conditions are that

$$U_z^{(1,R)} + U_z^{(1,S)} = U_z^{(2,T)} \quad \text{at } x=0 \tag{3.14}$$

and that $\sigma_{xz}^{(1)} = \sigma_{xz}^{(1)}$. Using $\sigma_{xz} = \mu(\partial u_z/\partial x)$, this entails

$$\mu_1 \frac{\partial U_z^{(1,R)}}{\partial x} + \mu_1 \frac{\partial U_z^{(1,S)}}{\partial x} = \mu_2 \frac{U_z^{(2,T)}}{\partial x} \quad \text{at } x=0. \tag{3.15}$$

Operating in Laplace space, it is easy to show that these conditions lead to [9]

$$U_{1,R} = \frac{\mu_1\beta_1 - \mu_2\beta_2}{\mu_1\beta_1 + \mu_2\beta_2} U_{1,S}\, \mathrm{e}^{-s\beta_1(x+x_0)} \tag{3.16}$$

and

$$U_{2,T} = \frac{2\mu_1\beta_1}{\mu_1\beta_1 + \mu_2\beta_2} U_{1,S}\, \mathrm{e}^{-s(\beta_2 x + \beta_1 x_0)}. \tag{3.17}$$

Of interest here is the inversion of the fundamental solution to the reflected wave problem, which gives rise to the image force. The inversion of $U_{1,R}$ can be performed via Cagniard–de Hoop, as in the previous section. The term to invert is

$$\mu_1 U_{1,R}(x,\lambda,s) = \frac{\mu_1\beta_1 - \mu_2\beta_2}{\mu_1\beta_1 + \mu_2\beta_2} \frac{\mathrm{e}^{-s(t_0 - \lambda y_0 - \beta_1 x_0)}}{2\beta_1}. \tag{3.18}$$

The first inversion, in x, is

$$\mu_1 \hat{u}_{1,R}(x,y,s) = \mathrm{e}^{-st_0} \frac{1}{2\pi \mathrm{i}} \int_{-\mathrm{i}\infty}^{\mathrm{i}\infty} \frac{\mu_1\beta_1 - \mu_2\beta_2}{\mu_1\beta_1 + \mu_2\beta_2} \frac{1}{2\beta_1} \mathrm{e}^{-s(\lambda(y-y_0) + \beta_1(x+x_0))}\, \mathrm{d}\lambda, \tag{3.19}$$

where, letting $\tilde{x} = x + x_0$, $\tilde{y} = y - y_0$, one can define a Cagniard path given by $\tau = \lambda\tilde{y} + \beta_1\tilde{x}$, i.e. such that

$$\lambda_{\pm}^{(1)} = \frac{\tau\tilde{y} \pm \mathrm{i}\tilde{x}\sqrt{\tau^2 - b_1^2\tilde{r}^2}}{\tilde{r}^2} \tag{3.20}$$

where $\tilde{r}^2 = \tilde{x}^2 + \tilde{y}^2$, and the superindex (1) is used to emphasize that λ depends on b_1 (i.e. that it corresponds to phase 1.

Equation (3.20) defines a hyperbola in the $\lambda^{(1)}$-plane, parametrized by $\tilde{x}$ and $\tilde{y}$ (or τ). Two branches are defined, one for $\tilde{y} > 0$ when $\mathrm{Re}[\lambda^{(1)}] < 0$ and one for $\tilde{y} < 0$ when $\mathrm{Re}[\lambda^{(1)}] > 0$; for brevity, here I focus on the $\tilde{y} < 0$ case (i.e. the positive half $\lambda^{(1)}$-plane), which is what is depicted on figure 5. The vertex of the two hyperbola branches are accordingly located at $\lambda = \mp b_1\tilde{y}/\tilde{r}$ for $\tau = b_1|\tilde{r}|$.

The integration path on equation (3.21) runs along the imaginary $\lambda^{(1)}$-axis; this integration path may be connected to either of the hyperbola branches via circumferential segments at infinity, thereby forming a closed contour of integration. Provided that no poles or branch cuts are left inside the contour, Cauchy's theorem may be invoked to show that the contour integral vanishes. Invoking Jordan's lemma, the integral along the circumferential segments at infinity needs to vanish as well, which thereby proves that the integral along the imaginary axis must be of the same value as that along the hyperbola branch. This is advantageous because the hyperbola branch maps into a line integral from $\tau = b_1\tilde{r}$ to $\tau \to \infty$ in the real τ-plane, which enables writing equation (3.21) in its Cagniard form.

However, the integrand in equation (3.21) has branch cuts starting at $\lambda_A^{(1)} = \pm b_1$, which can therefore be avoided, and at $\lambda_B^{(1)} = \pm b_2$, which may or may not be entirely avoidable depending on whether $b_2 > b_1$ or not. In the event that $b_2 < b_1$, the branch cut cannot be avoided for $t > t_p$,

Downloaded from https://royalsocietypublishing.org/ on 04 March 2022

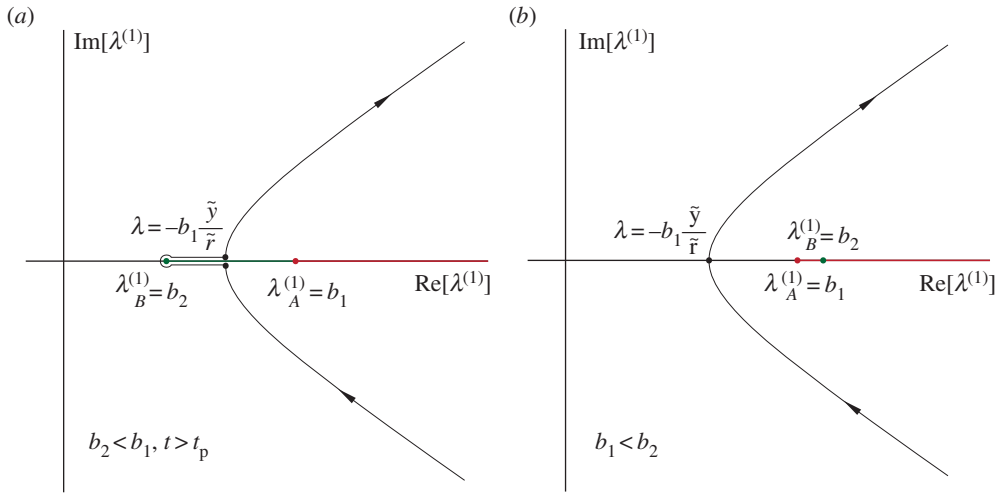

Figure 5. Integration paths depending on the relative values of μ_1, ρ_1 and μ_2, ρ_2. The branch cuts are represented in colour. (Online version in colour.)

where

$$t_p = -b_2 y \pm x\sqrt{b_1^2 - b_2^2}.$$

The resulting integration paths are depicted in figure 5. In addition, the integrand has poles at $\lambda_{p1}^{(1)} = b_1$ (coinciding with the branch cut, which is therefore entirely avoidable), and at

$$\lambda_{p2}^{(1)} = \pm\sqrt{\frac{b_1^2\mu_1^2 - b_2^2\mu_2^2}{\mu_1^2 - \mu_2^2}}.$$

Depending on the relative value of μ_1, ρ_1 and μ_2, ρ_2, this pole may contribute to the integration path. If $b_1 < b_2$ and $\mu_2 < \mu_1$, then the pole falls along the imaginary axis, and must be avoided by surrounding it; the same happens if $b_2 < b_1$ and $\mu_2 > \mu_1$. If $b_1 < b_2$ and $\mu_2 > \mu_1$, the pole falls along the real axis but prior to $\lambda_B^{(1)}$, so it will leave a residue; the same goes if $b_1 > b_2$ when $\mu_2 < \mu_1$.

The most immediate solution arises if the integration path need not be distorted beyond the hyperbola Cagniard path (i.e. either if $t < t_p$ with $b_2 < b_1$, or if entirely $b_1 > b_2$). In that case, the integration path is as described in figure 5*b*, and

$$\mu_1 \hat{u}_{1,R}(x, y, s) = \mathrm{e}^{-st_0}\frac{1}{\pi}\int_{+\tilde{r}b_1}^{\infty} \mathrm{Im}\left[\frac{\mu_1\beta_1 - \mu_2\beta_2}{\mu_1\beta_1 + \mu_2\beta_2}\frac{1}{2\beta_1}\frac{\partial\lambda^{(1)}}{\partial\tau}\right]\mathrm{e}^{-s\tau}\,\mathrm{d}\tau. \tag{3.21}$$

Upon taking the inverse in time via the Bromwich integral

$$\mu_1 u_{1,R}(x, y, t) = \frac{1}{2\pi\mathrm{i}}\int_{\mathrm{Br}}\left[\mathrm{e}^{-st_0}\frac{1}{\pi}\int_{+\tilde{r}b_1}^{\infty} \mathrm{Im}\left[\frac{\mu_1\beta_1 - \mu_2\beta_2}{\mu_1\beta_1 + \mu_2\beta_2}\frac{1}{2\beta_1}\frac{\partial\lambda^{(1)}}{\partial\tau}\right]\mathrm{e}^{-s\tau}\,\mathrm{d}\tau\right]\mathrm{e}^{-st}\,\mathrm{d}t \tag{3.22}$$

and invoking the properties of the Laplace transform, one finally obtains

$$\mu_1 u_{1,R}(x + x_0, y - y_0, t - t_0) = \frac{1}{\pi}\mathrm{Im}\left[\frac{\mu_1\beta_1 - \mu_2\beta_2}{\mu_1\beta_1 + \mu_2\beta_2}\frac{1}{2\beta_1}\frac{\partial\lambda^{(1)}}{\partial\tilde{t}}\right]H(\tilde{t} - b_1\tilde{r}), \tag{3.23}$$

where $\tilde{t} = t - t_0$. The explicit form of $u_{1,R}$ is given in appendix A.

In the event $t > t_p$ with $b_2 > b_1$, the integration path needs to be distorted as shown in figure 5. Upon changing the sign of x, there will be an additional contribution to the integral along the real axis, for real values of $\lambda^{(1)}$ and $\tau \in (t_p, b_1\tilde{r})$. Accordingly, there will be an additional contribution

Downloaded from https://royalsocietypublishing.org/ on 04 March 2022

of the form

$$\mu_1 u_{1,R}^{t_p}(x+x_0, y-y_0, t-t_0) = \frac{1}{\pi}\mathrm{Im}\left[\frac{\mu_1\beta_1-\mu_2\beta_2}{\mu_1\beta_1+\mu_2\beta_2}\frac{1}{2\beta_1}\frac{\partial\lambda^{(1)}}{\partial\tilde{t}}\right](H(\tilde{t}-t_p)-H(\tilde{t}-b_1\tilde{r})). \tag{3.24}$$

Given that in this case $\tilde{t} < b_1\tilde{r}$, $\lambda^{(1)} = \tilde{r}^{-2}(-\tau\tilde{y}+\tilde{x}\sqrt{b_1^2\tilde{r}^2-\tau^2})$, this may be rewritten as

$$\mu_1 u_{1,R}(x+x_0, y-y_0, t-t_0) = \frac{1}{\pi}\mathrm{Re}\left[\frac{\mu_1\beta_1-\mu_2\beta_2}{\mu_1\beta_1+\mu_2\beta_2}\frac{1}{2\beta_1}\frac{\partial\lambda^{(1)}}{\partial\tilde{t}}\right](H(\tilde{t}-t_p)-H(\tilde{t}-b_1\tilde{r})) \tag{3.25}$$

and retain the same expression of $\lambda^{(1)}$ as before. Appendix A provides an explicit expression of this term.

The possible poles entailed by the denominator $\mu_1\beta_1+\mu_2\beta_2$ do not contribute to the integration path. When $b_1 < b_2$ and $\mu_2 < \mu_1$ (or when $b_2 < b_1$ and $\mu_2 > \mu_1$), they are located along the imaginary axis at

$$\pm\lambda_{\mathrm{im}} = \pm\mathrm{i}\frac{b_2^2\mu_2^2-b_1^2\mu_1^2}{\mu_1^2-\mu_2^2}.$$

If the integration path along the imaginary axis is distorted to avoid them via two additional semi-circumferences $\Gamma_{\epsilon,\pm}$ of radius $\epsilon \to 0$, each located about $\pm\lambda_{\mathrm{im}}$, then making the change of variable $\lambda = \mp\lambda_{\mathrm{im}} + r\,\mathrm{e}^{\mathrm{i}\theta}$

$$\begin{aligned}
&\lim_{\epsilon\to 0}\int_{\Gamma_{\epsilon,\pm}} \frac{\mu_1\sqrt{b_1^2-\lambda^2}-\mu_2\sqrt{b_1^2-\lambda^2}}{(\lambda+\lambda_{\mathrm{im}})(\lambda-\lambda_{\mathrm{im}})}\mathrm{e}^{-s\left(x\sqrt{b_1^2-\lambda^2}-\lambda y\right)}\,\mathrm{d}\lambda \\
&= \int_{-\pi/2}^{\pi/2}\frac{1}{\pm 2\lambda_{\mathrm{im}}}\left[\left(\mu_1\sqrt{b_1^2-\lambda_{\mathrm{im}}^2}-\mu_2\sqrt{b_2^2-\lambda_{\mathrm{im}}^2}\right)\mathrm{e}^{\lambda_{\mathrm{im}}sy-sx\sqrt{b_1^2-\lambda_{\mathrm{im}}^2}}\right]\mathrm{d}\theta \\
&= \pm\frac{\pi}{2\lambda_{\mathrm{im}}}\left[\left(\mu_1\sqrt{b_1^2-\lambda_{\mathrm{im}}^2}-\mu_2\sqrt{b_2^2-\lambda_{\mathrm{im}}^2}\right)\mathrm{e}^{\lambda_{\mathrm{im}}sy-sx\sqrt{b_1^2-\lambda_{\mathrm{im}}^2}}\right],
\end{aligned} \tag{3.26}$$

so that each pole's contribution is of opposite sign, and it vanishes upon summing one with the other. Equally, the case where the pole is located along the real axis but before $\lambda_B^{(1)}$ does not leave a residue.

Thus, the fundamental solution for the reflected wave is given by

$$g_z(x+x_0, y-y_0, t-t_0) = \mu_1(u_{1,R}+u_{1,R}^{t_p}). \tag{3.27}$$

(b) Image force calculation for a injected, quiescent screw dislocation

As stated when defining equation (3.5), the fundamental solution is the system's response to a unit point force. Here, I am concerned with a screw dislocation, which in §2a was defined via a displacement boundary condition of the form

$$u_z(x,y,t) = \frac{B}{2}H(x-l)H(t)\delta(y), \tag{3.28}$$

where here the dislocation is injected at position $x = l$ to accommodate it to the coordinate system shown in figure 4.

In order to employ the fundamental solution derived above, one needs to express this displacement boundary condition in terms of its body force equivalent of the displacement boundary condition is given, in the sense of distributions, by [10]

$$f_z(x,y,t) = \frac{B}{2}H(x-l)H(t)\delta'(y), \tag{3.29}$$

where $\delta'(y) = \partial\delta(y)/\partial y$.

Downloaded from https://royalsocietypublishing.org/ on 04 March 2022

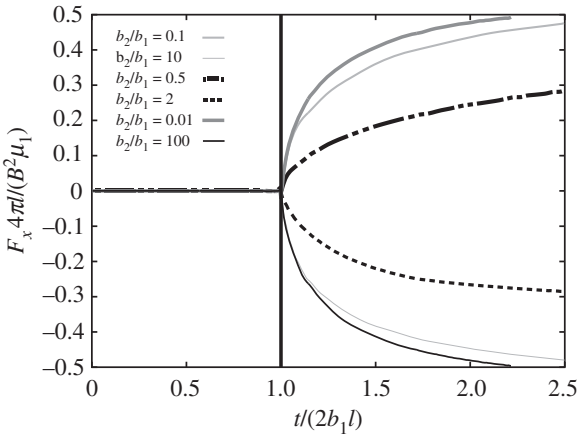

Figure 6. Image force for a screw dislocation in the presence of a dual phase interface. The vertical line at $t = 2b_1 l$ marks the onset of the response. For simplicity in the plot, it has been assumed that $\rho_1 = \rho_2$, so that $b_2/b_1 = \mu_1/\mu_2$. Note how the free surface case is recovered as $b_2/b_1 \to 0$, and the rigid interface case as $b_2/b_1 \to \infty$.

The reflected displacement due to the dislocation will therefore be

$$u_z^{(1,R)}(x,y,t) = \int_{-\infty}^{\infty} \mathrm{d}t_0 \int_{\mathbb{R}\times\mathbb{R}} \frac{B}{2} H(x_0 + l) H(t_0) \delta'(y_0) g_z(x - x_0, y - y_0, t - t_0)\, \mathrm{d}x_0\, \mathrm{d}y_0$$
$$= \frac{B}{2} \int_0^{\infty} \left[\int \frac{\partial}{\partial y} g_z(x, y, t - t_0)\, \mathrm{d}x \right]_{x \mapsto l - x} \mathrm{d}t_0, \tag{3.30}$$

where the sifting properties of the delta function, its derivative, and the step function have been used.

The σ_{zy} stress component of interest here, in turn, will be

$$\sigma_{zy}^{(1)}(x,y,t) = \frac{\mu_1 B}{2\pi} \frac{\partial}{\partial y} \int_0^{\infty} \left[\int \frac{\partial}{\partial y} g_z(x, y, t - t_0)\, \mathrm{d}x_0 \right]_{x \mapsto l - x} \mathrm{d}t_0. \tag{3.31}$$

The corresponding image force, evaluate at $x = -l$, $y = 0$, is

$$F_x(t) = \frac{\mu_1 B^2}{2\pi} \frac{\partial}{\partial y} \int_0^{\infty} \left[\int \frac{\partial}{\partial y} g_z(x, y, t - t_0)\, \mathrm{d}x \right]_{x = 2l,\ y = 0} \mathrm{d}t_0. \tag{3.32}$$

The asymptotic limit when $t \to \infty$ of this expression renders the elastostatic image force for these situations

$$\lim_{t\to\infty} F_x(t) = \lim_{t\to\infty} \frac{\mu_1 B}{2\pi} \frac{\partial}{\partial y} \int_0^{\infty} \left[\int \frac{\partial}{\partial y} g_z(x, y, t - t_0)\, \mathrm{d}x_0 \right]_{x \mapsto l - x} \mathrm{d}t_0$$
$$= \frac{\mu_1 B^2}{4\pi} \frac{\mu_2 - \mu_1}{\mu_2 + \mu_1} \frac{1}{l}. \tag{3.33}$$

It is also immediate to check that when $b_2/b_1 \to 0$ the case of an infinitely rigid interface solved in §2a is recovered; equally, when $b_2/b_1 \to \infty$ the case of a free surface is recovered.

A lengthy, but closed-form expression of this expression is given in appendix A, in terms of elliptic integrals of the first kind. The image force is plotted in figure 6. As in the rigid interface's case, the resulting image force is zero until the reflected wave scattered by the interface reaches the dislocation at $t = 2b_1 l$. Thereafter its magnitude increases steadily towards the asymptotic limit given in equation (3.33). As shown in figure 6, the image force remains repulsive if $b_2 > b_1$ (and $\mu_2 < \mu_1$), whereas it becomes attractive if $b_2 < b_1$ (and $\mu_2 > \mu_1$). The image force tends to converge to its asymptotic value faster if the values of b_2 and b_1 are similar.

Downloaded from https://royalsocietypublishing.org/ on 04 March 2022

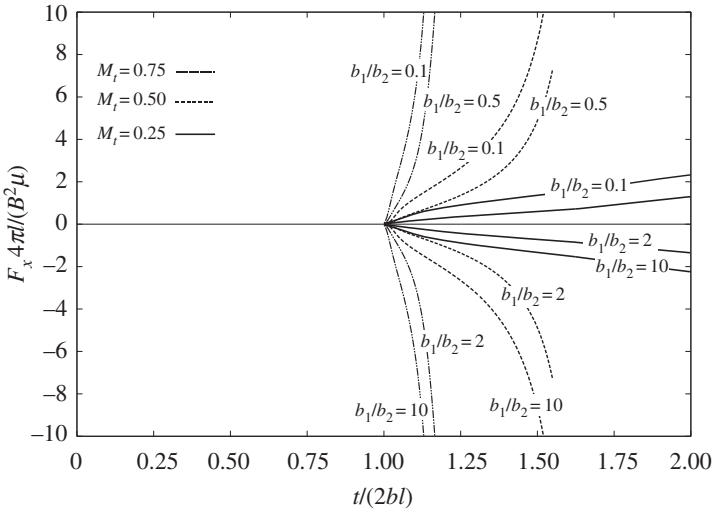

Figure 7. Image force for a screw dislocation uniformly gliding towards a dual phase interface. For simplicity in the plot, it has been assumed that $\rho_1 = \rho_2$, so that $b_2/b_1 = \mu_1/\mu_2$. Here $M_t = v/c_{t_1}$.

(c) Moving screw dislocation: two phases

This case may also be obtained from the convolution of the body force equivalent to the screw dislocation with the fundamental solution for the reflected wave obtained in §3a. The body force equivalent in this case is

$$f_z(x, y, t) = \frac{B}{2} H(x - (l(t) - l))H(t)\delta'(y), \tag{3.34}$$

whereupon the reflected displacement field in this case will be

$$u_z(x, y, t) = \frac{B}{2} \int_0^\infty \mathrm{d}t_0 \int_{\mathbb{R}} \frac{\partial}{\partial y} g_z(x_0 - (l(t) + l), y, t - t_0)\, \mathrm{d}x_0 \tag{3.35}$$

and

$$F_x(t) = \frac{B^2}{2\pi} \int_0^\infty \int_{-\infty}^\infty \frac{\partial^2}{\partial y^2} g_z(l - x_0, y, t - t_0)\bigg|_{y=0} \mathrm{d}t_0\, \mathrm{d}x_0. \tag{3.36}$$

The uniformly moving dislocation's case may be recovered setting $l(t) = v \cdot t$. Figure 7 shows the resulting image force values for different ratios b_1/b_2 and different constant glide speeds, attained by numerical integration of equation (3.36). As can be see in the figure, the image force tends to increase in magnitude over time, and unlike the quiescent cases, it does not saturate to its static counterpart: it tends to diverge as the dislocation approaches the interface. The dynamic magnification of the image force is stronger the larger the difference between b_1 and b_2 is, bracketed in between the two limiting cases of the infinitely rigid interface and the free surface (the free surface solutions can be found in [5]). It is worth pointing out that within $t = 4bl$, the magnitude of the image forces for dislocations moving at 25% of the transverse speed of sound (approx. 700 m s^{-1} in most metals) is doubled relative to the one predicted by elastostatic. Although it is not represented in the figure, at glide speeds of the order of $M_t = 0.03$ (i.e. ≈100 m s^{-1} in most metals), the magnitude of the force is doubled within $t \approx 7bl$. This entails that even for low speed dislocations, elastodynamic predicts considerably stronger image forces than those predicted in elastostatics.

Downloaded from https://royalsocietypublishing.org/ on 04 March 2022

4. Conclusion

This article has derived the expressions for the elastodynamic image forces of screw dislocations in the presence of a rigid boundary and two welded halfspaces of different material constants. Both the case of a injected, quiescent (non-moving) and the case of the non-uniformly moving dislocation have been studied. It has been shown that the rigid interface case may be solved using Head's image dislocation constructions but that, generally, the bimaterial case cannot be tackled with it due to wave scattering across the interface. For this case, the fundamental solution to the antiplane bimaterial solid has been explicitly derived, and then used in combination with the force representation of the screw dislocation, both moving and injected, to achieved closed-form solutions to the image force problem. The bimaterial case lies in-between the two asymptotic limits of the free surface and the rigid surface; depending on the ratio of elastic constants across the interface, the dislocation may be attracted towards (if $b_2 < b_1$) or repelled by (if $b_1 > b_2$) the interface. The quiescent dislocation's case tends to converge towards the elastostatic solution, but displays retardation effects related to the arrival time and reflection of the elastic wave from the rigid boundary. The moving dislocation's image force is also affected by retardation, but it has been shown not to converge to the elastotatic solution: it tends to diverge in magnitude as the dislocation approaches the interface, and well before that happens the magnitude of the image force is seen to surpass the one predicted in elastostatics. This *dynamic magnification* effect is brought about by the Doppler-like effect the elastodynamic field of the dislocation displays in its motion: ahead of the dislocation core and in the direction of motion, the magnitude of the elastic field is stronger [8]; because it is this component of the field that reaches the interface first and is subsequently reflected (thereby giving rise to the image force), the image force itself is magnified. Therefore, the effect is not related to the fact that in its motion towards the surface the dislocation is increasingly closer to the interface, but to the asymmetric nature of the elastodynamic fields, brought about by inertial effects displayed by moving dislocations. Crucially, it has been shown that the dynamic magnification effect is strong even at very low glide speeds, quickly surpassing the elastostatic prediction's magnitude.

This effect, that extends from the free surface case to the rigid boundary case, suggests that careful consideration must be given to dynamic effects affecting dislocations approaching phase boundaries: the image forces they are subjected to are much larger than predicted by elastostatics over timescales and glide speed ranges that are of relevance even to low strain rate dislocation mediated processes. The significance of this finding and its potential impact is dual, as it demarcates a crucial distinction in the way image force constructions ought to be employed. On the one hand, the equilibrium configuration of dislocations in the presence of interfaces (such as those brought about by misfit and threading dislocations in layered materials), where dislocations achieve specific lattice positions in order to accommodate misfit strains along the interface, may still be treated via elastostatics, so long as the dislocations affected by the image forces do not contribute to the plastic slip of the material. On the other hand, however, if dislocations move in the presence of an interface, as could be the case in the presence of shear bands or martensitic bands, the conventional treatment of image forces as elastostatic will likely prove to underestimate the magnitude of the image forces, which could be corrected employing the expressions provided in this work.

The current derivations may immediately be extended to the study of screw dislocations with cut surfaces along any general direction. Furthermore, the results in §3 may be employed to study further antiplane shear phenomena such as wave reflections by mode III cracks. However, a more general treatment is required for the study of general loading problems. Future work will focus on deriving analogous expressions for the edge dislocation, and on exploring the effect multiple phase boundaries have on the findings of this article.

Data accessibility. This article has no additional data.

Competing interests. I declare I have no competing interests.

Funding. The author was financially supported by the Master and Fellows of Trinity College, University of Cambridge under the author's Title A Fellowship.

Acknowledgements. B.G.-L. acknowledges the support of the Master and Fellows of Trinity College Cambridge.

Downloaded from https://royalsocietypublishing.org/ on 04 March 2022

Appendix A

The form of the displacement field's fundamental solution is

$$u_{1,R} = -\frac{\mu_2^2(A_1^2+A_2^2)(x^2+y^2)+\mu_1^2(b_1^2y^2-t^2)}{2\pi\sqrt{t^2-b_1^2(x^2+y^2)}(\mu_2^2(A_1^2+A_2^2)(x^2+y^2)+2\mu_1\mu_2\left(A_1tx+A_2y\sqrt{t^2-b_1^2(x^2+y^2)}\right)+\mu_1^2(t^2-b_1^2y^2))}$$

and

$$u_{1,R}^{tp} = \frac{\mu_1\mu_2(A_2tx-A_1y\sqrt{b_1^2-(x^2+y^2)-t^2}}{\pi\sqrt{b_1^2(x^2+y^2)-t^2}\left(\mu_2^2(A_1^2+A_2^2)(x^2+y^2)+2\mu_1\mu_2\left(A_1tx+A_2y\sqrt{b_1^2(x^2+y^2)-t^2}\right)+\mu_1^2(t^2-b_1^2y^2)\right)},$$

where

$$A_1 = \sqrt[4]{\frac{(-b_1^2y^2+b_2^2(x^2+y^2)+t^2)^2}{(x^2+y^2)^2}-\frac{4b_2^2t^2x^2}{(x^2+y^2)^2}} \times \cos\left(\frac{1}{2}\tan^{-1}\left(\frac{2txy\sqrt{t^2-b_1^2r^2}}{r^4(-b_1^2y^2/r^2+b_2^2-t^2x^2/r^4+t^2y^2/r^4)}\right)\right)$$

and

$$A_2 = \sqrt[4]{\frac{(-b_1^2y^2+b_2^2(x^2+y^2)+t^2)^2}{(x^2+y^2)^2}-\frac{4b_2^2t^2x^2}{(x^2+y^2)^2}} \times \sin\left(\frac{1}{2}\tan^{-1}\left(\frac{2txy\sqrt{t^2-b_1^2r^2}}{r^4(-b_1^2y^2/r^2+b_2^2-t^2x^2/r^4+t^2y^2/r^4)}\right)\right).$$

For $x = 2l$, the injected image force of the quiescent dislocation

$$\begin{aligned}
F_x(t) = {} & \frac{1}{105(b_1-b_2)^3(b_1+b_2)^3t^2x^7\sqrt{t^2-b_1^2x^2}\sqrt{t^2+(b_2^2-b_1^2)x^2}} \\
& \times\Bigg(-160t^{10}-160\sqrt{t^2+(b_2^2-b_1^2)x^2}t^9+496b_1^2x^2t^8-248b_2^2x^2t^8 \\
& +416b_1^2x^2\sqrt{t^2+(b_2^2-b_1^2)x^2}t^7-168b_2^2x^2\sqrt{t^2+(b_2^2-b_1^2)x^2}t^7-686b_1^4x^4t^6-274b_2^4x^4t^6 \\
& +1036b_1^2b_2^2x^4t^6-498b_1^4x^4\sqrt{t^2+(b_2^2-b_1^2)x^2}t^5-210b_2^4x^4\sqrt{t^2+(b_2^2-b_1^2)x^2}t^5 \\
& +784b_1^2b_2^2x^4\sqrt{t^2+(b_2^2-b_1^2)x^2}t^5+420b_1^6x^6t^4-234b_2^6x^6t^4+1168b_1^2b_2^4x^6t^4 \\
& -2030b_1^4b_2^2x^6t^4-8\mathrm{i}(13b_1^6+68b_2^2b_1^4-23b_2^4b_1^2+6b_2^6)\sqrt{-\frac{b_1^2}{t^2}}x^7 \\
& \times\sqrt{1-\frac{b_1^2x^2}{t^2}}\sqrt{\frac{(b_2^2-b_1^2)x^2}{t^2}+1}E\left(\mathrm{i}\sinh^{-1}\left(\sqrt{-\frac{b_1^2}{t^2}}x\right)\middle|1-\frac{b_2^2}{b_1^2}\right)t^4 \\
& +8b_2^2(59b_1^4+2b_2^2b_1^2+3b_2^4)\mathrm{i}x^7F\left(\mathrm{i}\sinh^{-1}\left(\sqrt{-\frac{b_1^2}{t^2}}x\right)\middle|1-\frac{b_2^2}{b_1^2}\right)\sqrt{-\frac{b_1^2}{t^2}}\sqrt{\frac{(b_2^2-b_1^2)x^2}{t^2}+1} \\
& \cdot\sqrt{1-\frac{b_1^2x^2}{t^2}}t^4+283b_1^6x^6\sqrt{t^2+(b_2^2-b_1^2)x^2}t^3-105b_2^6x^6\sqrt{t^2+(b_2^2-b_1^2)x^2}t^3 \\
& +525b_1^2b_2^4x^6\sqrt{t^2+(b_2^2-b_1^2)x^2}t^3-1379b_1^4b_2^2x^6\sqrt{t^2+(b_2^2-b_1^2)x^2}t^3+34b_1^8x^8t^2-48b_2^8x^8t^2
\end{aligned}$$

Downloaded from https://royalsocietypublishing.org/ on 04 March 2022

$$
\begin{aligned}
&+ 466b_1^2b_2^6x^8t^2 - 1622b_1^4b_2^4x^8t^2 + 1682b_1^6b_2^2x^8t^2 + 840b_1^4b_2^2x^6\sqrt{t^2+(b_2^2-b_1^2)x^2}\sqrt{t^2-b_1^2x^2}t^2 \\
&+ 420b_1^4b_2^2x^6\log\left(\sqrt{t^2+(b_2^2-b_1^2)x^2}+\sqrt{t^2-b_1^2x^2}\right)\sqrt{t^2+(b_2^2-b_1^2)x^2}\sqrt{t^2-b_1^2x^2}t^2 \\
&+ 420b_1^4b_2^2x^6\log\left(t+\sqrt{t^2-b_1^2x^2}\right)\sqrt{t^2+(b_2^2-b_1^2)x^2}\sqrt{t^2-b_1^2x^2}t^2 \\
&- 41b_1^8x^8\sqrt{t^2+(b_2^2-b_1^2)x^2}t + 105b_1^2b_2^6x^8\sqrt{t^2+(b_2^2-b_1^2)x^2}t - 315b_1^4b_2^4x^8\sqrt{t^2+(b_2^2-b_1^2)x^2}t \\
&+ 763b_1^6b_2^2x^8\sqrt{t^2+(b_2^2-b_1^2)x^2}t - 104b_1^{10}x^{10} + 48b_1^2b_2^8x^{10} - 232b_1^4b_2^6x^{10} \\
&\left.+ 728b_1^6b_2^4x^{10} - 440b_1^8b_2^2x^{10}\right), \qquad \text{(A 1)}
\end{aligned}
$$

where $F(\cdot\,|\,\cdot)$ is an elliptic integral of the first kind and $E(\cdot\,|\,\cdot)$ of the second kind.

References

1. Hirth JP, Lothe J. 1982 *Theory of dislocations*, 2nd edn. New York, NY: John Wiley & Sons.
2. Matthews JW, Blakeslee AE. 1975 Defects in epitaxial multilayers: II. Dislocation pile-ups, threading dislocations, slip lines and cracks. *J. Cryst. Growth* **29**, 273–280. (doi:10.1016/0022-0248(75)90171-2)
3. Elsner J, Jones R, Sitch PK, Porezag VD, Elstner M, Frauenheim Th, Heggie MI, Öberg S, Briddon PR. 1997 Theory of threading edge and screw dislocations in GaN. *Phys. Rev. Lett.* **79**, 3672–3675. (doi:10.1103/PhysRevLett.79.3672)
4. Head AK. 1953 The interaction of dislocations and boundaries. *Philos. Mag. Ser. 7* **44**, 92–94. (doi:10.1080/14786440108520278)
5. Gurrutxaga-Lerma B, Balint DS, Dini D, Sutton AP. 2015 Elastodynamic image forces on dislocations. *Proc. R. Soc. A* **471**, 20150433. (doi:10.1098/rspa.2015.0433)
6. Verschueren J, Gurrutxaga-Lerma B, Balint DS, Dini D, Sutton AP. 2017 The injection of a screw dislocation into a crystal: atomistics versus continuum elastodynamics. *J. Mech. Phys. Solids.* **98**, 366–389. (doi:10.1016/j.jmps.2016.10.004)
7. Markenscoff X. 1980 The transient motion of a nonuniformly moving dislocation. *J. Elast.* **10**, 193–201. (doi:10.1007/BF00044503)
8. Gurrutxaga-Lerma B, Balint DS, Dini D, Eakins DE, Sutton AP. 2013 A dynamic discrete dislocation plasticity method for the simulation of plastic relaxation under shock loading. *Proc. R. Soc. A* **469**, 20130141. (doi:10.1098/rspa.2013.0141)
9. Achenbach JD. 1973 *Wave propagation in elastic solids*. New York, NY: North-Holland.
10. Burridge R, Knopoff L. 1964 Body force equivalents for seismic dislocations. *B. Seismol. Soc. Am.* **54**, 1875–1888.